A LuGre Tire Friction Model with Exact Aggregate Dynamics

Panagiotis Tsiotras*, Efstathios Velenis* and Michel Sorine**

Abstract— **The LuGre dynamic point contact friction model for the two-dimensional translation of a body on a surface has been used in the past to derive a model for the friction forces and moments at the contact patch of a tire. The resulting tire friction model is distributed, described by a set of partial differential equations. Several approximations have been used in the literature to approximate this distributed model using a set of ordinary differential equations, making the model appropriate for control design and on-line estimation. In this paper the method of moments is used to derive a set of ordinary differential equations to describe the exact average dynamics of the distributed model. Three cases of normal load distribution are considered and compared: uniform, trapezoidal and cubic load distribution. Simulations are also presented to compare with existing approximate steady-state lumped models.**

I. Introduction

In the past several years, the problem of modeling and predicting tire friction has become an area of intense research in the automotive community. Knowledge of the friction characteristics is necessary for the development of control systems such as the ABS, TCS, ESP, etc. which have enhanced safety and maneuverability of modern wheeled vehicles.

Recently, a new class of tire friction models has been developed that capture the dynamic behavior of friction forces–the so-called "dynamic tire friction models". A model for the longitudinal friction forces of a tire, based on dynamic elastoplastic friction model is presented in [1] and extended to the longitudinal/lateral motion in [2], [3]. Slightly different in spirit is the work in [4] where a static map of relative velocity to friction and the dynamics of slip and slip angle were used to predict tire friction forces, by taking into consideration the effects of length relaxation.

The longitudinal LuGre tire friction model, initially introduced in [5] and later corrected and improved upon in [6] and [7], was based on a dynamic visco-elastoplastic friction model for point contact initially introduced in [8]. The LuGre tire friction model for combined longitudinal/lateral motion first appeared in [9], [10].

In [11] the LuGre tire friction model for combined longitudinal/lateral motion was developed taking into account all aspects neglected in [9], [10], that is, coupling of the forces in longitudinal and lateral directions (neglected in [9]), tire anisotropy (neglected in [10]) and rim rotation (neglected in both [9] and [10]). In addition, a solid mathematical justification for the introduction of dynamic friction models based on fundamental physical properties of the friction forces, such as dissipativity and maximality of the dissipation rate, as in [12], was provided.

The major advantage of the LuGre dynamic tire friction model compared to the one of [2], [3] is its simpler lumped form. The term *lumped form* refers to the model's description by a set of ordinary differential equations. Both models in [2], [3] and the LuGre tire friction model were derived initially as distributed models described by a partial differential equation. The lumped model in [2], [3] was derived using a finite element approach, resulting in a system with a potentially large number of states. In [9], [10], [11] the lumped LuGre tire model for longitudinal/lateral motion was derived by introducing the mean states along the length of the contact patch, the behavior of which can be described by a system of three ordinary differential equations. These equations give the forces and aligning moment at the contact patch of the tire. The lumped form makes the model more suitable for the development and implementation of on-line estimation and control algorithms [13], [14]. The main objective of the lumped model in [9], [10], [11] was to capture the steady-state behavior of the distributed model exactly. Therefore, the lumped LuGre model in [9], [10], [11] does not offer any guarantees on the accuracy of the transient behavior when compared to the distributed model.

In this paper, the derivation of the lumped LuGre tire model is revisited, this time using the method of moments formulation [15], [16] and captures the exact dynamics of the distributed model. This allows one to validate the assumptions used in the literature for the derivation of simpler, low order, steady-state lumped models. In the first section of this paper the distributed LuGre tire model is reviewed. Next, the essential definitions of the method of moments are provided and the exact lumped model is derived for three specific cases of normal load distribution, namely, uniform, trapezoidal and cubic distribution. At the end of the paper numerical simulations are presented to compare the dynamic behavior of the simplified low order lumped models of [9], [10], [11] with the aggregate dynamics of the distributed model.

II. The Distributed LuGre Dynamic Tire Friction Model

The distributed LuGre tire friction model for combined longitudinal/lateral motion was derived in [11] by applying the point contact LuGre friction model (for the two-dimensional translation of a body on a surface) on the contact patch of a tire. In order to take into consideration the fact that undeformed tire elements enter the contact

* School of Aerospace Engineering, Georgia Institute of Technology, Atlanta, GA 30332-0150, USA, {p.tsiotras,efstathios_velenis}@ae.gatech.edu

** INRIA Rocquencourt, Domaine de Voluceau, B.P. 105, 78153 Le Chesnay Cedex, FRANCE, michel.sorine@inria.fr

0-7803-8335-4/04/$17.00 ©2004 AACC

patch as the tire rotates, the contact patch was divided into infinitesimal stripes $\mathrm{d}\zeta$ along the length of the contact patch (Fig. 1). The point contact model was then applied to the tire elements in each of the infinitesimal stripes resulting in a distributed model described by a set of partial differential equations, with time t and longitudinal position on the patch ζ being the independent variables.

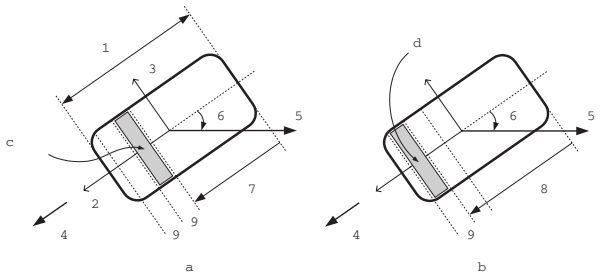

Fig. 1. Frame of reference and velocities at the contact patch. Derivation of the distributed tire model.

The distributed tire model is summarized in the following equations [11]

$$\begin{aligned}\frac{\mathrm{d}z_i(t,\zeta)}{\mathrm{d}t} &= \frac{\partial z_i(t,\zeta)}{\partial t} + |\omega r|\frac{\partial z_i(t,\zeta)}{\partial \zeta} \\ &= v_{ri}(t) - C_{0i}(v_r)z_i(t,\zeta),\ i=x,y \quad (1)\\ \mu_i(t,\zeta) &= -\sigma_{0i}z_i(t,\zeta) - \sigma_{1i}\frac{\partial z_i(t,\zeta)}{\partial t} \\ &\quad -\sigma_2 v_{ri}(t),\quad i=x,y \quad (2)\\ F_i(t) &= \int_0^L \mu_i(t,\zeta)f_n(\zeta)\mathrm{d}\zeta,\quad i=x,y \quad (3)\\ M_z(t) &= -\int_0^L \mu_y(t,\zeta)f_n(\zeta)\left(\frac{L}{2}-\zeta\right)\mathrm{d}\zeta \quad (4)\end{aligned}$$

By $z_i(t,\zeta),\ i=x,y$, we denote the internal friction states [11] which correspond to the elastic deformations of the tire element at time t and position ζ on the contact patch, along the longitudinal x and lateral y directions. In accordance to the above discussion, the boundary condition for equations (1) is $z_i(t,0)=0$. That is, the tire fiber is undeflected as it enters the patch. The constants $\sigma_{0i},\ i=x,y$, correspond to the stiffness of the tire elements in the x and y directions, while σ_{1i} and σ_{2i} are damping constants for the friction coefficient $\mu_i(t,\zeta)$. The functions $C_{0i}(v_r)$ characterize the steady-state characteristics of the model. For more details the reader is referred to [11]. For a tire with the same static friction characteristics along the longitudinal and lateral directions, as the one considered in [10], the $C_{0i}(v_r)$ function is given by

$$C_{0i}(v_r) = \frac{|v_r|\sigma_{0i}}{g(v_r)}\ ,\quad i=x,y \quad (5)$$

where,

$$g(v_r) = \mu_k + \big(\mu_s-\mu_k\big)e^{-\left(\frac{|v_r|}{v_s}\right)^{\gamma}}. \quad (6)$$

In (6) μ_k and μ_s denote the kinetic and static Coulomb friction coefficients, respectively, and v_s denotes the Stribeck characteristic velocity [8]. The parameter γ is used to achieve desirable steady-state behavior of the tire friction [7].

The function $f_n(\zeta)$ in (3) denotes the normal load distribution along the contact patch. The relative velocity components of the contact patch with respect to the road $v_{ri},\ (i=x,y)$, appear as inputs to the system of equations (1)-(4) and are given by

$$\begin{aligned}v_{rx} &= \omega r - v\cos(\alpha), \quad (7)\\ v_{ry} &= -v\sin(\alpha), \quad (8)\end{aligned}$$

where ω is the angular rate of the tire and r its radius. By v we denote the magnitude of the translational speed of the wheel and by α the slip angle (Fig. 1). By v_r we denote the vector sum of v_{rx} and v_{ry}, and thus $|v_r| = \sqrt{v_{rx}^2 + v_{ry}^2}$. The output of the model is the longitudinal $F_x(t)$ and lateral $F_y(t)$ friction forces at the center of the patch as well as the aligning moment $M_z(t)$.

In the following sections we present a methodology for expressing the *exact* dynamics of the distributed model (1)-(4) by a set of *ordinary differential equations* instead of the partial differential equation (1), for several special cases of the normal load distribution $f_n(\zeta)$.

III. Exact Lumped Model Using the Method of Moments

Define the pth moment of $z_i(t,\zeta)$ for $\zeta\in[a\ \ b]$ as follows

$$M_{p,i}^{ab}(t) := \int_a^b z_i(t,\zeta)\zeta^p\mathrm{d}\zeta,\quad i=x,y \quad (9)$$

Taking the time derivative of $M_{p,i}^{ab}$ yields,

$$\begin{aligned}\dot{M}_{p,i}^{ab}(t) &= \int_a^b \frac{\partial z_i(t,\zeta)}{\partial t}\zeta^p\mathrm{d}\zeta \\ &\quad -|\omega r|\int_a^b \frac{\partial z_i(t,\zeta)}{\partial \zeta}\zeta^p\mathrm{d}\zeta. \quad (10)\end{aligned}$$

Integrating by parts, (10) gives a recursive formula for the calculation of all moments $M_{p,i}^{ab}$ for $p\geq 1$

$$\begin{aligned}\dot{M}_{p,i}^{ab} &= \frac{b^{p+1}-a^{p+1}}{p+1}v_{ri} - C_{0i}(v_r)M_{p,i}^{ab} \\ &\quad -|\omega r|z_i(t,\zeta)\zeta^p\Big|_a^b + |\omega r|pM_{p-1,i}^{ab} \quad (11)\end{aligned}$$

For $p=0$ (11) gives

$$\begin{aligned}\dot{M}_{0,i}^{ab} &= (b-a)v_{ri} - C_{0i}(v_r)M_{0,i}^{ab} \\ &\quad -|\omega r|\Big(z_i(t,b)-z_i(t,a)\Big) \quad (12)\end{aligned}$$

Given any normal load distribution $f_n(\zeta)$, we can approximate f_n with a Taylor series as follows

$$f_n(\zeta) \simeq \sum_{k=0}^{m} c_k\zeta^k \quad (13)$$

for some constants $c_0, c_1, ..., c_m$. Note that the total normal load on the contact patch is given by

$$F_n = \int_0^L f_n(\zeta)\mathrm{d}\zeta. \tag{14}$$

Using the moments $M_{p,i}^{ab}$, the friction forces $F_i(t),\ i = x, y$ in (3) can be written as follows

$$F_i(t) = -\sigma_{0i}\sum_{k=0}^{m} c_k M_{k,i}^{0L} - \sigma_{1i}\sum_{k=0}^{m} c_k \dot{M}_{k,i}^{0L} - \sigma_{2i} v_{ri} F_n$$

Finally, the aligning torque $M_z(t)$ in (4) can be written in terms of the moments $M_{p,i}^{ab}$ as

$$\begin{aligned} M_z(t) &= -\frac{L}{2}F_y(t) + \sigma_{2y} v_{ry}\int_0^L f_n(\zeta)\zeta\mathrm{d}\zeta \\ &\quad +\sigma_{0y}\sum_{k=0}^{m} c_k M_{k+1,y}^{0L} + \sigma_{1y}\sum_{k=0}^{m} c_k \dot{M}_{k+1,y}^{0L} \end{aligned}$$

A. Closure Relationship

Equations (11), (12) require the time history of the internal friction states $z_i(t,\zeta)$ for fixed positions on the contact patch $\zeta = \zeta_0$, namely, $\zeta_0 = a$ and $\zeta_0 = b$. In this section we discuss the calculation of these terms.
Going back to the original partial differential equation (1) let us consider the characteristics given by

$$t = t(s)\ ,\quad \zeta = \zeta(s)\ ,\quad \text{with}\ \ \frac{\partial \mathrm{t}}{\partial \mathrm{s}} = 1\ ,\quad \frac{\partial \zeta}{\partial \mathrm{s}} = |\omega \mathrm{r}|.$$

Let the characteristic $y(s) = \zeta(t(s))$ starting from $\zeta = 0$ at time $t - \tau$ for some (still unknown) τ and ending at $\zeta = \zeta_0$ at time t. Then

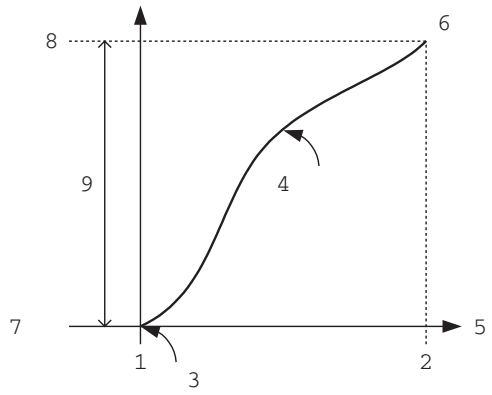

Fig. 2. Solution $z_i(t,\zeta)$ along the characteristic $y(s) = \zeta(t(s))$.

$$y(\bar{t}) = \int_{t-\tau}^{\bar{t}} |\omega r|(\sigma)\mathrm{d}\sigma \tag{15}$$

and $y(t) = \zeta_0$. Hence,

$$\zeta_0 = \int_{t-\tau}^{t} |\omega r|(\sigma)\mathrm{d}\sigma \tag{16}$$

Let us follow the solution along the characteristic (Fig. 2). To this end, define $\xi_i(t) := z_i(t, y(t))$. Thus,

$$\dot{\xi}_i(t) = \frac{\partial z_i}{\partial t} + \frac{\partial z_i}{\partial y}\frac{\partial y}{\partial t} = v_{ri} - C_{0i}(v_r)\xi_i(t) \tag{17}$$

with initial condition

$$\xi_i(t-\tau) = z_i(t-\tau, y(t-\tau)) = z_i(t-\tau, 0) = 0\ .$$

Finally, $z_i(t,\zeta_0) = \xi_i(t)$ and τ is such that (16) holds.

IV. The Effect of Normal Force Distribution

A. Exact Lumped Model for Uniform Load Distribution

The uniform load distribution $f_n(\zeta) = c_0$ is derived from (13) with $m = 0$ while in equations (11) and (12) we substitute $a = 0$ and $b = L$. The dynamics of friction are described by five ordinary differential equations with states $M_{0,x}^{0L}$, $M_{0,y}^{0L}$ from equation (12), $M_{1,y}^{0L}$ from equation (11) with $p = 1$ and $z_x(t,L)$, $z_y(t,L)$ from equation (17). A methodology for choosing realistic initial conditions is discussed in Section IV-D.

B. Exact Lumped Model for Trapezoidal Load Distribution

In order to reproduce realistic aligning moment characteristics a non-symmetric normal load distribution should be used. In [10] a trapezoidal normal load distribution was introduced. In this case the function $f_n(\zeta)$ is given by

$$f_n(\zeta) = \begin{cases} C_1\zeta & \text{for} \quad 0 \le \zeta \le \alpha, \\ f_{\max} & \text{for} \quad \alpha \le \zeta \le \beta, \\ C_2\zeta + C_3 & \text{for} \quad \beta \le \zeta \le L. \end{cases} \tag{18}$$

The normal load distribution above is only piecewise smooth. In this case, it is necessary to define different moments of $z_i(t,\zeta)$ for different areas of the contact patch, i.e. $M_{p,i}^{0\alpha}(t)$ for $\zeta \in [0\ \alpha]$, $M_{p,i}^{\alpha\beta}(t)$ for $\zeta \in (\alpha\ \beta)$ and $M_{p,i}^{\beta L}(t)$ for $\zeta \in [\beta\ L]$. Thus, the dynamics of friction are described by a set of nineteen ordinary differential equations with states $z_i(t,\alpha)$, $z_i(t,\beta)$ and $z_i(t,L)$, $M_{0,i}^{0\alpha}$, $M_{0,i}^{\alpha\beta}$ and $M_{0,i}^{\beta L}$ from equation (12), $M_{1,i}^{0\alpha}$ and $M_{1,i}^{\beta L}$ from equation (11), with $i = x, y$ and finally $M_{2,y}^{0\alpha}$, $M_{1,y}^{\alpha\beta}$ and $M_{2,y}^{\beta L}$ again from equation (11). The calculation of $z_i(t,\alpha)$, $z_i(t,\beta)$ and $z_i(t,L)$ is done in accordance to the discussion of Section III-A using equation (17). The choice of initial conditions is discussed in Section IV-D.
The lumped forces are now given by

$$\begin{aligned} F_i(t) &= -\sigma_{2i} v_{ri} F_n \\ &\quad -\sigma_{0i}\left(C_1 M_{1,i}^{0\alpha} + f_{\max} M_{0,i}^{\alpha\beta} + C_2 M_{1,i}^{\beta L} + C_3 M_{0,i}^{\beta L}\right) \\ &\quad -\sigma_{1i}\left(C_1 \dot{M}_{1,i}^{0\alpha} + f_{\max} \dot{M}_{0,i}^{\alpha\beta} + C_2 \dot{M}_{1,i}^{\beta L} + C_3 \dot{M}_{0,i}^{\beta L}\right) \end{aligned} \tag{19}$$

and the aligning torque by

$$\begin{aligned} M_z(t) &= -\frac{L}{2}F_y + \sigma_{2y} v_{ry}\int_0^L f_n(\zeta)\zeta\mathrm{d}\zeta \\ &\quad +\sigma_{0y}\left(C_1 M_{2,y}^{0\alpha} + f_{\max} M_{1,y}^{\alpha\beta} + C_2 M_{2,y}^{\beta L} + C_3 M_{1,y}^{\beta L}\right) \\ &\quad +\sigma_{1y}\left(C_1 \dot{M}_{2,y}^{0\alpha} + f_{\max} \dot{M}_{1,y}^{\alpha\beta} + C_2 \dot{M}_{2,y}^{\beta L} + C_3 \dot{M}_{1,y}^{\beta L}\right) \end{aligned} \tag{20}$$

C. Exact Lumped Model for a Cubic Load Distribution

In this section we introduce another approximation for the normal load distribution at the contact patch. The cubic normal load distribution (Fig. 3) is derived from (13) for $m = 3$:

$$f_n(\zeta) = c_3\zeta^3 + c_2\zeta^2 + c_1\zeta + c_0 \tag{21}$$

Using this approximation, one is able to incorporate the effects of the pneumatic trail, resulting in realistic aligning torque predictions, as well as the natural boundary conditions of the normal load distribution, i.e. $f_n(\zeta = 0) = f_n(\zeta = L) = 0$. In addition, the proposed expression is smooth along the whole length of the contact patch and the pth moment of $z_i(t,\zeta)$ from $\zeta = 0$ to $\zeta = L$, $M^{0L}_{p,i}$, may be used. Thus, we avoid splitting the integral (10) as was done for the trapezoidal distribution. This also results in a smaller number of states (and differential equations).

It can be easily shown that in this case the dynamics of the tire friction are described by a set of eleven ordinary differential equations with states $z_x(t,L)$ and $z_y(t,L)$ from equation (17), $M^{0L}_{p,x}$ and $M^{0L}_{p,y}$ with $p = 0, 1, ..., 3$ from equations (11) and (12) and $M^{0L}_{4,y}$ from equation (11). Once again, the choice of initial conditions is discussed in Section IV-D.

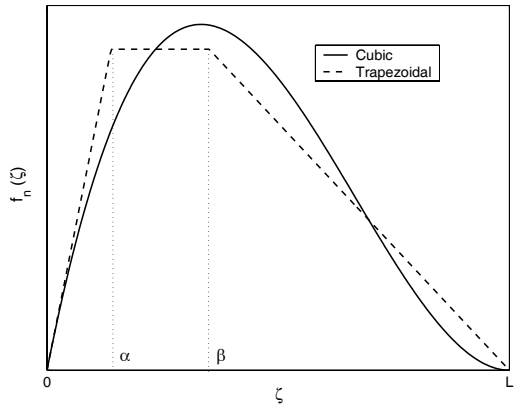

Fig. 3. Trapezoidal and Cubic normal load distributions

D. Initial Conditions

The initial condition $\xi_i(0) = z_i(0,\zeta_0)$ in (17) can be calculated easily by integrating (17) from $t = -\tau$ to $t = 0$, where

$$\tau = \frac{\zeta_0}{|\omega r|}. \tag{22}$$

Under the assumption that during this period v, ω and α are constant, one obtains

$$\xi(t=0) = \frac{v_{ri}}{C_{0i}(v_r)}\left(1 - e^{-C_{0i}(v_r)\tau}\right) \tag{23}$$

Substituting τ from (22) in (23) one obtain

$$\xi(t=0) = \frac{v_{ri}}{C_{0i}(v_r)}\left(1 - e^{-\frac{C_{0i}(v_r)\zeta_0}{|\omega r|}}\right) = z_i(0,\zeta_0) \tag{24}$$

The same result can be obtained by assuming that the tire is initially at steady-state with constant ω, v and α. To this end, we may enforce $\frac{\partial z_i(t,\zeta)}{\partial t} = 0$ in equation (1) to obtain

$$\frac{\partial z_i(t,\zeta)}{\partial \zeta} = \frac{1}{|\omega r|}\Big(v_{ri} - C_{0i}(v_r) z_i(t,\zeta)\Big), \quad i = x, y \tag{25}$$

Taking into consideration the boundary condition $z_i(t,0) = 0$ (no deflection at the entry point of the contact patch) and the steady-state conditions of constant ω, v and α, we may integrate (25) to obtain the distribution $z_i^{ss}(\zeta)$ of z_i $(i = x, y)$, along the contact patch length at steady-state, as in [10] and [11].

$$z_i^{ss}(\zeta) = \frac{v_{ri}}{C_{0i}(v_r)}\left(1 - e^{-\frac{C_{0i}(v_r)\zeta}{|\omega r|}}\right), \quad i = x, y \tag{26}$$

For $\zeta = \zeta_0$ the previous expression coincides with (24).

We use the expression (26), equivalently (24), in (9) to calculate the initial conditions $M^{ab}_{pi}(0)$ for all the moment equations (11), (12).

V. Numerical Simulations

In this section we present numerical simulations of the previously developed lumped LuGre tire friction models [9], [10], [11] and compare the results with the exact lumped model developed in this paper. The tire friction models under consideration are subject to the same excitation consisting of a linearly decreasing angular rate ω (from $32\,\mathrm{rad/sec}$ to $0\,\mathrm{rad/sec}$ in $2\,\mathrm{sec}$) and constant velocity $v = 8\,\mathrm{m/sec}$ and slip angle $\alpha = 4^o$ (Fig. 1). It is noted that although such an excitation is not realistic for passenger vehicles under normal operating conditions, nonetheless it can be reproduced experimentally in a laboratory environment[1].

A. Uniform Normal Load Distribution

In [10] two approximate lumped LuGre tire friction models were developed. These models are summarized in the equations below:

$$\dot{\tilde{z}}_i(t) = v_{ri} - \left(C_{0i}(v_r) + \frac{\kappa_i}{L}|\omega r|\right)\tilde{z}_i(t) \tag{27}$$

$$F_i(t) = -F_n\left(\sigma_{0i}\tilde{z}_i + \sigma_{1i}\dot{\tilde{z}}_i + \sigma_{2i}v_{ri}\right), \; i = x, y \tag{28}$$

The two different lumped models are derived for different approximations of the κ_i term. This term is either approximated as a constant $\kappa_i \in [1.1 \;\; 1.4]$, or as a function of ω and v_r, $\kappa_i = \kappa_i^{ss}(v_r, \omega)$, such that the steady-state solution of the lumped model captures exactly the *steady-state* solution of the distributed model. The latter expression for κ_i is given by [10] as follows

$$\kappa_i^{ss} = \frac{1 - e^{-L/Z_i}}{1 - \frac{Z_i}{L}\left(1 - e^{-L/Z_i}\right)}, \quad Z_i = \frac{|\omega r|}{C_{0i}(v_r)} \tag{29}$$

It is shown in [10] that these approximate lumped models capture the steady-state characteristics of the distributed friction very well, while no guarantees for the accuracy

[1]The "Mobile Tire Tester" in [4] is such a device. It is used to validate tire friction models.

of the dynamic behavior were given. Evaluation of the dynamic behavior of the approximate lumped models is now possible via comparison with the exact lumped model presented in Section IV-A.

Two cases are investigated. The first one assumes low tire stiffness ($\sigma_{0i} = 150\ \mathrm{m}^{-1},\ i = x, y$), and the second one assumes higher tire stiffness ($\sigma_{0i} = 500\ \mathrm{m}^{-1},\ i = x, y$). The time histories of the friction forces (Fig. 4) show that the approximations made in [10] are more realistic when the stiffness of the tire is higher. In this case the steady-state is reached faster. As already mentioned, the approximate lumped models in [10], [11] were derived with the steady-state behavior accuracy in mind.

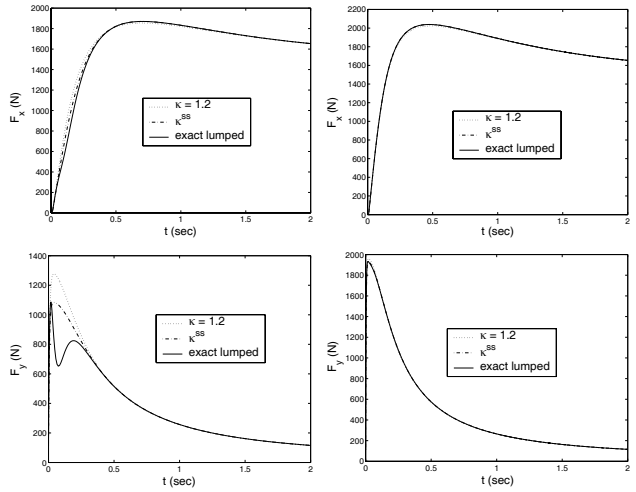

Fig. 4. Time histories for longitudinal and lateral forces (left column: $\sigma_{0i} = 150\ \mathrm{m}^{-1},\ \ i = x, y$, right column: $\sigma_{0i} = 500\ \mathrm{m}^{-1},\ \ i = x, y$)

B. Trapezoidal and Cubic Load Distribution

In [11] an approximate average lumped model was developed for the case of the trapezoidal normal load distribution. The dynamics of the friction forces are given by (27) and (28). In [11] the κ_i term was approximated by a function κ_i^{ss} such that the force prediction of the lumped model matches the ones of the distributed model at steady-state. The aligning torque predictions of the LuGre tire friction model with a trapezoidal normal load distribution are comparable to experimental data [10], [11] at steady-state. The dynamics of the aligning torque completing the approximate average lumped model [10], [11] are summarized below:

$$\begin{aligned}\dot{\hat{z}}_y(t) &= \frac{G}{F_n L} v_{ry} - C_{0y}\hat{z}_y(t) - \nu(t)|\omega r|\hat{z}_y(t) \\ &\quad + \frac{|\omega r|}{L}\bar{z}_y(t) \qquad (30)\\ M_z(t) &= F_n L\Big[\sigma_{0y}\left(\frac{1}{2}\tilde{z}_y - \hat{z}_y\right) + \sigma_{1y}\left(\frac{1}{2}\dot{\tilde{z}}_y - \dot{\hat{z}}_y\right) \\ &\quad + \sigma_{2y}\left(\frac{1}{2}v_{ry} - \frac{G}{F_n L}\right)\Big] \qquad (31)\end{aligned}$$

where $G = \int_0^L f_n(\zeta)\zeta \mathrm{d}\zeta$.

Similarly to the approximation of the κ_i term for the friction forces, the $\nu(t)$ term in (30) was approximated in [11] by a static function ν^{ss}, such that the aligning torque predictions of the average lumped model matches the ones of the distributed one at steady-state.

Next, we compare the dynamic behavior of the average lumped model developed in [11] with the ones presented in Sections IV-B and IV-C. In order to make a fair comparison between the trapezoidal and the cubic normal load distribution models, we have selected the parameters of the two different expressions (18) and (21) such that they produce the same total normal force F_n and the same longitudinal position of C.G. of the normal load distribution.

We consider the case of tire stiffness $\sigma_{0i} = 500\ \mathrm{m}^{-1},\ (i = x, y)$. The results are shown on the left column of Fig. 5. In Fig. 5 the time histories of the friction forces and aligning torque are shown. We observe that the three models converge to the same steady-state. We also observe, however, significant differences in the transient behavior of the three models which are more apparent in the lateral force F_y and aligning torque M_z.

This discrepancy is due to the fact that the normal load distribution $f_n(\zeta)$, along with the distribution of the contact patch deflection $z_i(t, \zeta)$, determine the amount of the total friction generated by each tire element along the contact patch length (see equations (2), (3)) at each time t. In the case of the approximate lumped model of [11] the use of the average states $\tilde{z}_i(t),\ i = x, y$ and $\hat{z}_y(t)$ averages the individual contribution of each tire element to the total friction, thus resulting in smoother transient behavior of the friction forces and aligning torque. On the other hand, in the case of the exact lumped model, the product of the individual contact patch deflection $z_i(t, \zeta)$, with $f_n(\zeta)$ determines the amount of friction generated by each tire element in the contact patch; see equations (2)-(3). This is true both for the distributed and the exact lumped models. In Fig. 3 we observe that the trapezoidal normal load distribution weights more the tire elements close to the contact patch entry point ($\zeta = 0$) compared to the cubic distribution. Observing the initial distribution of z_y^{ss} in Fig. 6 we notice that the tire elements close to $\zeta = 0$ are less deformed compared to tire elements for larger values of ζ. As ω is reduced however (for example, $\omega = 20$ rad/sec) the distribution of z_y^{ss} tends to a uniform one. As a result, it is expected that for the case of trapezoidal normal load distribution we should get lower lateral forces initially, but finally tending to the same values as the ones predicted by the cubic distribution model. This is in agreement with the results shown in Fig. 5.

To verify these observations, a second set of numerical simulations was performed, using the approximate model in [11] and the exact trapezoidal and cubic models of Sections IV-B, IV-C respectively, with the slip angle taken as $\alpha = 15^o$. The tire stiffness and the excitation remained the same. The results are shown in the right column of Figure 5. In this set of simulations the time histories of the

friction forces and the aligning moment is almost identical for all three cases of normal load distributions. The right plot in Fig. 6 reveals that for $\alpha = 15^o$ the distribution of z_y^{ss} is very close to a uniform one.

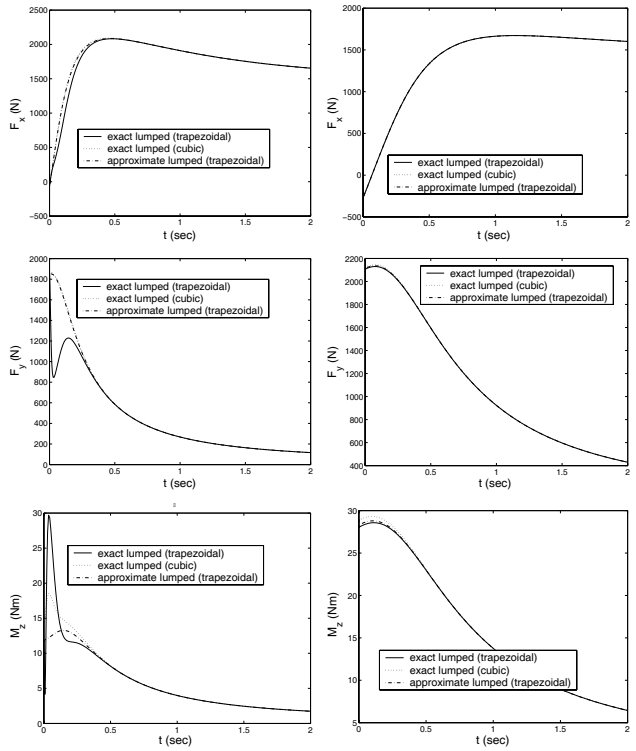

Fig. 5. Time histories for longitudinal/lateral forces and aligning torque (trapezoidal and cubic normal load distribution), left column: $\alpha = 4^o$, right column: $\alpha = 15^o$

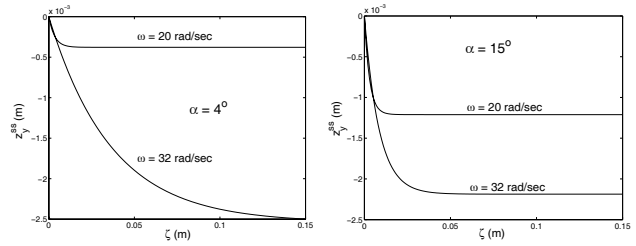

Fig. 6. Distribution of $z_y^{ss}(\zeta)$ along the contact patch, left column: $\alpha = 4^o$, right column: $\alpha = 15^o$

VI. Conclusions

A methodology to compute the *exact* dynamics of the aggregate distributed LuGre dynamic tire friction model by a set of ordinary differential equations is presented. The results of this work allow one to validate the assumptions considered in the development of the low-order approximate lumped models. A comparative analysis shows that, given a sufficiently high stiffness of the tire, the approximate models reproduce the dynamics of the aggregate distributed tire model very accurately.

Acknowledgment: The work of the first two authors was supported by the US Army Research Office, award no. DAAD19-00-1-0473.

References

[1] P. Bliman, T. Bonald, and M. Sorine, "Hysteresis operators and tyre friction models. application to vehicle dynamic simulation," in *Proceedings of ICIAM 95*, Hamburg, Germany, July 3-7 1995.

[2] M. Sorine and J. Szymanski, "A new dynamic multi d.o.f. tire model," in *Transportation Systems 2000*, Braunschweig, Germany, 2000.

[3] J. Szymansky, "Modèles réduits du contact pneu-sol et applications à l'automobile," Renault, Technocentre Renault, Guyancourt, France, Technical Report, 1999.

[4] P. Fancher, J. Bernard, C. Clover, and C. Winkler, "Representing truck tire characteristics in simulations of braking and braking-in-a-turn maneuvers," *Vehicle System Dynamics Supplement*, vol. 27, pp. 207–220, 1997.

[5] C. Canudas de Wit and P. Tsiotras, "Dynamic tire friction models for vehicle traction control," in *Proceedings of 38th IEEE Conference on Decision and Control*, Phoenix, Arizona, USA, 1999, pp. 3746–3751.

[6] J. Deur, "Modeling and analysis of longitudinal tire dynamics based on the LuGre friction model," Ford Motor Company, Scientific Research Laboratory MD 1170, Dearborn, MI 48121-2053, USA," Technical Report, 2001.

[7] C. Canudas de Wit, P. Tsiotras, E. Velenis, M. Basset, and G. Gissinger, "Dynamic friction models for road/tire longitudinal interaction," *Vehicle System Dynamics*, vol. 39, no. 3, pp. 189–226, 2003.

[8] C. Canudas de Wit, H. Olsson, K. J. Åström, and P. Lischinsky, "A new model for control of systems with friction," *IEEE Transactions on Automatic Control*, vol. 40, no. 3, pp. 419–425, 1995.

[9] X. Claeys, C. Canudas de Wit, J. Yi, R. Horowitz, L. Alvarez, and L. Richard, "A new 3d dynamic tire/road friction model for vehicle simulation and control," in *Proceedings of the ASME-IMECE World Conference*, New York, USA, November 2001.

[10] J. Deur, J. Asgari, and D. Hrovat, "A dynamic tire friction model for combined longitudinal and lateral motion," in *Proceedings of the ASME-IMECE World Conference*, New York, USA, November 2001.

[11] E. Velenis, P. Tsiotras, and C. Canudas-de Wit, "Extension of the lugre dynamic tire friction model to 2d motion," in *Proceedings of the 10th IEEE Mediterranean Conference on Control and Automation - MED2002*, July 9-12 2002, lisbon, Portugal.

[12] M. Sorine, "Applications of hysteresis models: Contact friction in tires, muscle contraction," in *IEEE CDC 98 Workshop #2*, Tampa, Florida, 1998.

[13] C. Canudas-de Wit, M. Petersen, and A. Shiriaev, "A new nonlinear observer for tire/road distributed contact friction," in *Proceedings of the 42^{th} IEEE Conference on Decision and Control*, Maui, Hawaii, 2003.

[14] C. Canudas de Wit, R. Horowitz, and P. Tsiotras, "Model-based observers for tire/road contact friction prediction," in *New Directions in Nonlinear Observer Design*, ser. Lecture Notes in Control and Information Science, H. Nijmeijer and T. Fossen, Eds. London: Springer-Verlag, 1999, vol. 244, pp. 23–42.

[15] N. Akhiezer, *The Classical Moment Problem*. New York: Hafner Publishing Company, 1965.

[16] G. Zahalak, "A comparison of the mechanical behavior of the cat soleus muscle with a distribution-moment model," *Transactions of the ASME Journal of Biomechanical Engineering*, vol. 108, pp. 131–140, 1986.